The Journal of Chemical Physics

RAPID COMMUNICATION | DECEMBER 22 2025

Unveiling the CO_2 hydrate phase diagram from computer simulation: Locating the hydrate–liquid–vapor coexistence and its upper quadruple point FREE

Special Collection: Carlos Vega Festschrift

Jesús Algaba ; Samuel Blazquez ; Cristóbal Romero-Guzmán ; Carlos Vega ; María M. Conde ; Felipe J. Blas

J. Chem. Phys. 163, 241101 (2025)
https://doi.org/10.1063/5.0307295

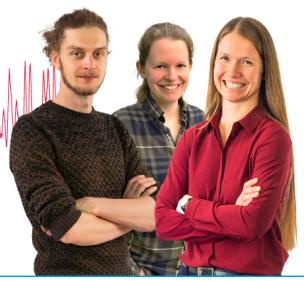

The Journal of Chemical Physics COMMUNICATION pubs.aip.org/aip/jcp

Unveiling the CO_2 hydrate phase diagram from computer simulation: Locating the hydrate–liquid–vapor coexistence and its upper quadruple point

Cite as: J. Chem. Phys. 163, 241101 (2025); doi: 10.1063/5.0307295
Submitted: 15 October 2025 • Accepted: 3 December 2025 •
Published Online: 22 December 2025

Jesús Algaba,[1] Samuel Blazquez,[2] Cristóbal Romero-Guzmán,[1] Carlos Vega,[2] María M. Conde,[3,a)] and Felipe J. Blas[1,a)]

AFFILIATIONS

[1] Laboratorio de Simulación Molecular y Química Computacional, CIQSO-Centro de Investigación en Química Sostenible and Departamento de Ciencias Integradas, Universidad de Huelva, 21006 Huelva, Spain
[2] Dpto. Química Física I, Fac. Ciencias Químicas, Universidad Complutense de Madrid, 28040 Madrid, Spain
[3] Departamento de Ingeniería Química Industrial y del Medio Ambiente, Escuela Técnica Superior de Ingenieros Industriales, Universidad Politécnica de Madrid, 28006 Madrid, Spain

Note: This paper is part of the Special Topic, Carlos Vega Festschrift.
[a)] **Authors to whom correspondence should be addressed:** maria.mconde@upm.es and felipe@uhu.es

ABSTRACT

Carbon dioxide (CO_2) hydrates hold promising applications in capturing and separating CO_2 for climate change mitigation. Understanding their behavior at the molecular level is, therefore, essential, and computer simulations have become powerful tools for exploring their formation and stability, providing valuable insights into their underlying mechanisms. In this work, we perform molecular dynamics simulations to compute the three-phase coexistence line involving the stability region where CO_2 is in the vapor phase: CO_2 hydrate–liquid water–vapor. This computation was previously inaccessible using the traditional three-phase direct coexistence technique. To achieve this, we employ a novel solubility-based method, which allows us to accurately evaluate the coexistence line. Our results exhibit excellent agreement with experimental data and, for the first time, accurately reproduce the hydrate–liquid–vapor equilibrium line of the CO_2–water phase diagram. Finally, we have determined the upper quadruple point (Q_2), where the four phases, namely hydrate, liquid water, liquid CO_2, and vapor, coexist. Our pioneering result for the Q_2 value shows remarkable agreement with experimental observations, validating the accuracy of our findings and representing a significant milestone in the field of gas hydrate research.

I. INTRODUCTION

Clathrate hydrates, or simply hydrates, are expected to play a central role in the global transition from fossil fuels to renewable energy sources.[1–9] These strategic materials are non-stoichiometric crystalline inclusion compounds formed by hydrogen-bonded water molecules (host) capable of encapsulating molecules of interest (guest) under appropriate thermodynamic conditions.[10,11] These compounds are of great interest because of their applications as a methane (CH_4) reservoir,[1,2] as a safe option for hydrogen (H_2) storage,[3,12,13] as a clean alternative for recovering nitrogen (N_2) from industrial gas emissions,[4,14] and as a stable method for CO_2 capture,[5–9,15] among others. The case of CO_2 hydrates is particularly relevant because of their significance in the context of global climate change.[10,11] In recent years, considerable effort has been devoted to developing viable strategies for the secure capture and storage of CO_2 to mitigate this pressing challenge, and the use of hydrates as molecular containers for CO_2 represents a promising, albeit technically demanding, approach. For these reasons, CO_2 hydrates have been extensively investigated through both experimental studies[9,15–22] and molecular simulations.[23–39]

Accurate knowledge of the thermodynamic stability of gas hydrates, particularly their phase diagrams, is crucial for their efficient utilization in energy production, carbon sequestration, gas storage, and transportation.[10,11] Phase diagrams delineate the conditions under which hydrates form and remain stable, thereby enabling the identification of optimal and cost-effective conditions for clathrate hydrate formation and application. Over the past several decades, extensive experimental studies have determined the hydrate dissociation line, which typically represents a three-phase equilibrium in a binary system, where hydrate, aqueous, and guest-rich gas or liquid phases coexist, depending on the identity of the guest molecule. Authoritative treatments of this subject can be found in the monograph by Sloan and Koh[10] and in the recent volume by Ripmeester and Alavi,[11] which provides a comprehensive review of hydrate phase behavior.

Molecular simulation offers a complementary route for determining hydrate dissociation lines.[10,11,40,41] In particular, the direct coexistence (DC) method introduced by Ladd and Woodcock[42,43] was successfully adapted to hydrate systems by some of us,[44,45] who first applied it to CH_4 hydrates. Since the initial work of Conde and Vega,[44] this approach has inspired numerous studies that have employed the DC method to determine the dissociation lines of various hydrates under different conditions.[23,24,26,38,39,44,46–55]

In a subsequent study, Tanaka and co-workers[56] determined the mutual solubilities of CH_4 in water under conditions where the aqueous solution coexists with both the CH_4 hydrate and the pure CH_4 phase. The solubilities were estimated from the excess chemical potential of the solute in the aqueous phase, assuming infinite dilution. This theoretical framework is among the standard approaches employed within classical equations of state to locate three-phase coexistence conditions involving gas and/or solid phases.[57–59] More recently, we have extended this methodology by computing solubilities directly from molecular simulations, thereby demonstrating that the so-called solubility method constitutes a distinct yet fully equivalent alternative to the DC approach for determining the CH_4 hydrate dissociation line.[60] This technique has later been applied by several authors to predict dissociation conditions,[28,53,61,62] including CO_2 hydrates.[28] In accordance with this innovative method, previously used to account for the hydrate–water–CO_2 three-phase line, the solubility of CO_2 when an aqueous phase (L_{H_2O}) is in contact with a vapor phase (L_{H_2O}–V) and when in contact with a hydrate phase (H–L_{H_2O}) is calculated keeping the pressure constant and exploring different temperatures. Under the three-phase coexistence conditions, the solubilities obtained from both equilibria (L_{H_2O}–V and H–L_{H_2O}) have to be the same, or in other words, the temperature at which the solubility curves intersect at constant pressure is the three-phase equilibrium temperature (T_3). The employed method has been schematized in Fig. 1, where we show snapshots of the H–L_{H_2O} (top left) and L_{H_2O}–V (top right) coexistences and their corresponding solubility curves (blue and red, respectively). As can be seen in the scheme, and as is well known, the solubility of a gas in water increases as the temperature decreases; however, in the case of hydrate–water systems, the behavior is the opposite. The intersection between those curves is the triple point temperature, where the three phases H–L_{H_2O}–V coexist (a snapshot of the three phases in coexistence is shown in Fig. 1 bottom). Indeed, the introduction of this novel approach and the results presented in the subsequent paragraphs signify a remarkable breakthrough in the field of research.

It is important to recall that Tanaka and collaborators[63,64] have recently determined the H–L_{H_2O}–V coexistence curve of the CO_2 hydrate by evaluating the chemical potentials of water and CO_2 along the hydrate–CO_2 and hydrate–water equilibrium boundaries, using the van der Waals–Platteeuw theory.[65,66] The intersection of these two lines defines the T_3 triple point. Although he also computes the hydrate–water and water–CO_2 solubilities, which could, in principle, be used to locate T_3, he chose to determine it through the chemical potential route. It should be noted that this approach is not a purely molecular simulation prediction, as it relies on the van der Waals–Platteeuw theoretical framework.[65,66]

Despite the recent contributions by Tanaka and co-workers and by other authors,[28,53,60–64] a critical gap persists in

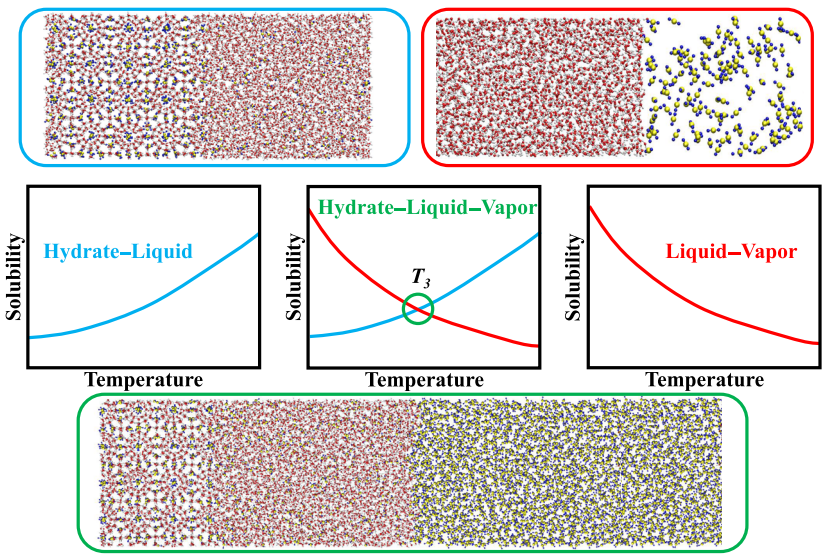

FIG. 1. Top left: Snapshot of the hydrate–liquid coexistence. Top right: Snapshot of the liquid–vapor coexistence. Middle: Schematic solubility of a gas as a function of temperature of an aqueous phase when in contact via a planar interface with a hydrate phase (left), a vapor phase (right), and in a triple coexistence (center). Bottom: Snapshot of the triple coexistence hydrate–liquid–vapor.

simulation-based studies: the accurate prediction of the hydrate–water–vapor coexistence line for systems containing guest molecules that can exist in both vapor and liquid phases, obtained solely from computer simulations without invoking any theoretical framework. To the best of our knowledge, all simulation studies about the CO_2 hydrate have been performed at pressures above 44.99 bar, at which the CO_2 + water binary mixture exhibits a H–L_{H_2O}–L_{CO_2} three-phase coexistence line, where the hydrate, aqueous, and liquid CO_2 phases coexist. At pressures below 44.99 bar, the liquid CO_2 phase becomes a vapor phase (V) and the system shows a H–L_{H_2O}–V three-phase equilibrium. Both three-phase coexistence lines (H–L_{H_2O}–V and H–L_{H_2O}–L_{CO_2}) meet at a Q_2 quadrupole point[10] at 283 K and 44.99 bar. Although several simulation studies have been dedicated to the study of the CO_2 hydrate phase diagram,[23,24,26,28] the study of the H–L_{H_2O}–V branched remains elusive.

From a molecular dynamics (MD) perspective, the problem in simulating the hydrate–water–vapor coexistence line arises from the inherently different nature of the phases involved. While the water and hydrate phases have comparable densities and compressibilities, allowing them to be modeled effectively under constant pressure (NPT) conditions, the vapor phase presents a much lower density and significantly higher compressibility. In particular, the density of the CO_2 vapor phase is about one order of magnitude lower, and the compressibility is about an order of magnitude higher. It means that usual algorithms fail to keep the pressure constant when a condensed phase and a vapor phase coexist in the same simulation box. This difference causes barostats in MD simulations to struggle with maintaining stable pressure, especially when all three phases are present in the simulation box.[67] At this point, it is important to remark that both methods, DC and the original solubility method, present the same problem due to the vapor nature of the CO_2 phase. In fact, when the DC technique is applied to systems containing vapor phases, the barostat often struggles to equilibrate properly and to yield accurate pressure values.

When the DC technique is employed to determine the H–L_{H_2O}–V equilibrium line at low pressures, below the Q_2 of the CO_2 hydrate, the method artificially extends the H–L_{H_2O}–L_{CO_2} three-phase line. This occurs because it fails to correctly reproduce the vapor phase—the system pressure does not equilibrate properly—thereby pushing the coexistence line into a metastable region and yielding an incorrect slope in the guest vapor region.

The topology of the phase diagram exhibited by CO_2 hydrate is not unique. Many other clathrate hydrates display similar features, whereas some systems exhibit distinctly different topologies. For hydrates formed from a single guest species, two general types of phase diagrams can be identified depending on the critical temperature (T_c) of the guest. When T_c lies near or below the triple-point temperature of pure water, the phase diagram differs topologically from that of guests whose T_c exceeds the water triple point.[10]

For guests with relatively low T_c, the region of interest for hydrate formation does not involve a liquid phase of the guest, whose behavior remains effectively gas-like. Under these conditions, only the hydrate–liquid–vapor (H–L_{H_2O}–V) three-phase line exists. This line extends from higher temperatures and pressures toward lower values and terminates at a quadruple point (commonly denoted Q_1 in the literature), where several three-phase lines intersect, all involving ice I_h as one of the coexisting phases.[10] This behavior is characteristic of CH_4 and N_2 hydrates. The less dense phase is conventionally labeled as V (vapor), although it is, strictly speaking, a supercritical fluid, since the conditions relevant to hydrate formation typically lie above the guest's critical point. For CH_4 and N_2 hydrates, the density of the gas-like phase is sufficiently high that it is more appropriately described as a fluid rather than a true vapor. In particular, CH_4 hydrate does not exhibit the equilibration issues discussed above, since the CH_4-rich fluid under H–L_{H_2O}–V coexistence conditions possesses a mass density approximately one-half to one-third that of pure water. Under these conditions, the barostat employed in the DC technique performs reliably.

In contrast, guests whose T_c exceeds the triple point of water exhibit phase diagrams with a different topology. In the hydrate-forming region, the guest condenses to form a distinct liquid (L) phase. In this case, in addition to the H–L_{H_2O}–V three-phase line, a further hydrate–liquid–liquid (H–L_{H_2O}–L_{guest}) three-phase line appears. Here, L_{guest} denotes a guest-rich liquid phase (L_{CO_2} in the case of the CO_2 hydrate). Systems of this type are hereafter referred to as liquid-like. The H–L_{H_2O}–L_{guest} line extends from higher temperatures and pressures toward lower values and terminates at an upper quadruple point (denoted Q_2), where hydrate, water-rich liquid, guest-rich liquid, and vapor coexist. From this Q_2 point, the H–L_{H_2O}–V line continues toward lower temperatures and pressures until it meets the Q_1 quadruple point.[10] Such liquid-like behavior is typical of ethane (C_2H_6), hydrogen sulfide (H_2S), and CO_2, among others.[10] As previously discussed for CO_2 hydrate, the H–L_{H_2O}–V three-phase line cannot be accurately determined using the standard DC technique, as the vapor phase is not dense enough compared to the water-rich liquid phase for the barostat to operate properly.

In this work, we demonstrate that an extension of the recently proposed solubility-based method enables accurate calculation of the three-phase coexistence equilibrium in CO_2 hydrate systems. Using this innovative approach, we report—for the first time—the H–L_{H_2O}–V three-phase equilibrium (hydrate–water–CO_2 vapor) and the upper Q_2 quadruple point of the CO_2–water phase diagram, where four distinct phases coexist: CO_2 hydrate, liquid water, liquid CO_2, and vapor. Among the various hydrates that exhibit gas- and liquid-like behavior, we select CO_2 hydrate since it is one of the most extensively studied.[10,11] Its relevance to carbon capture and sequestration has led to a wealth of experimental data, making it an ideal benchmark system for testing the accuracy of molecular dynamics simulations.

The remainder of this paper is organized as follows: Section II presents the molecular models and simulation details. The results and their discussion are given in Sec. III, and the conclusions are summarized in Sec. IV.

II. MOLECULAR MODELS AND SIMULATION DETAILS

In this work, water and CO_2 molecules are represented using the widely adopted TIP4P/Ice[68] and TraPPE[69] force fields, respectively. This combination has been previously employed in the literature to determine the three-phase coexistence curve of CO_2 hydrates.[23,26,28,38,39] Míguez *et al.*[23] proposed a modification of the unlike water–CO_2 interactions by introducing a scaling factor $\xi = 1.13$ such that $\varepsilon_{W\text{–}CO_2} = 1.13(\varepsilon_{W\text{–}W}\,\varepsilon_{CO_2\text{–}CO_2})^{1/2}$, where $\varepsilon_{W\text{–}W}$

and $\varepsilon_{CO_2-CO_2}$ are the water–water and CO_2–CO_2 Lennard-Jones dispersive interactions. Notice that the factor 1.13 is applied to the interaction of water with both the C and O atoms of the CO_2 molecule. This adjusted combination rule yields an accurate description of the CO_2 hydrate dissociation temperature along the entire three-phase coexistence line.[23,28,38,39]

Unfortunately, although this combination of the TIP4P/Ice water model, the CO_2 model, and the selected ξ value performs well for the H–L_{H_2O}–L_{CO_2} three-phase equilibrium, it does not reproduce CO_2 solubilities with the same accuracy. The TIP4P/Ice model with $\xi = 1.13$ systematically overestimates experimental CO_2 solubilities.[23] However, as will be explained later, our aim is not to determine solubility values themselves, but rather to identify the T_3 point, which corresponds to the intersection of the two solubility curves.

All MD simulations have been performed using GROMACS (2021.5).[70] In all cases, the Verlet-leapfrog algorithm[71] with a time step of 2 fs was used for solving Newton's dynamic equations, as well as a cutoff, for the dispersive and Coulombic interactions, of 1.0 nm. Following our previous studies,[23,28,38,39] the Berthelot combining rule has been modified for the water–CO_2 interactions as $\varepsilon_{W-CO_2} = \xi(\varepsilon_{W-W}\ \varepsilon_{CO_2-CO_2})^{1/2}$, with $\xi = 1.13$. Long-range corrections were not applied to the LJ part of the potential. The smooth PME[72,73] method was used to account for long-range electrostatic interactions. In addition, PME[72,73] (particle mesh Ewald) long-range corrections were applied for the Coulombic interactions. We have employed the Nosé–Hoover thermostat[74] algorithm with a coupling time constant of 2 ps to fix the temperature. In the case of *NPT* simulations, an anisotropic Parrinello–Rahman barostat[75] with a coupling time constant of 2 ps was used to fix the pressure and avoid stress from the solid hydrate structure.

III. RESULTS

Following the solubility method,[28,53,56,60–62] previously explained, the three-phase coexistence equilibrium problem can be split into two coexistence equilibria of two phases (V–L_{H_2O} and H–L_{H_2O}). We first focus on the case of V–L_{H_2O} equilibria, in which the pressure cannot be kept constant due to the difference in density and compressibility of the V and L_{H_2O} phases. Since the pressure cannot be fixed to a desired constant value, the *NVT* canonical ensemble is the most appropriate ensemble for a system with a vapor–liquid (V–L_{H_2O}) interface.[40,41] Although the pressure cannot be fixed, there is still a method to obtain the solubility under the desired temperature and pressure conditions. V–L_{H_2O} *NVT* simulations of 400 ns (100 ns for the equilibration and 300 ns for the production period) can be carried out at constant temperature but varying the volume and/or the number of molecules in the simulation box. We have fixed the number of water molecules at 4000 in all cases, but the number of molecules of CO_2 has been fixed at 300 and 600. The top-right snapshot of Fig. 1 depicts the L_{H_2O}–V simulation setup, with the water-rich liquid phase (L_{H_2O}) located on the left side of the simulation box and a planar interface separating it from the vapor phase (V) on the right. The z side of the simulation box (L_z), which is the direction along the V–L interface, has been extended from 40 to 180 nm (L_x and L_y have a fixed value of 2.8 nm). Keeping the temperature constant at 270, 275, 280, and 285 K, the different combinations of L_z values and CO_2 molecules—see Table I—allow us to explore the V–L_{H_2O} system at pressures ranging from 5 to 50 bar.

TABLE I. Values of pressures calculated from the *NVT* simulations as a function of the number of molecules of CO_2 (N_{CO_2}) and the dimension of the z side (L_z) of the simulation box. In all cases, the number of molecules of water was 4000, and L_x and L_y were fixed to 2.8 nm.

T (K)		270	275	280	285
L_z (nm)	N_{CO_2}		P (bar)		
180	300	6.76(1)	7.11(1)	7.57(1)	7.85(1)
120	300	8.79(1)	9.41(2)	9.61(1)	10.52(1)
180	600	14.66(2)	15.47(2)	15.69(2)	16.82(2)
120	600	18.11(3)	19.20(3)	20.08(3)	20.83(3)
80	600	23.68(3)	25.16(3)	26.42(4)	27.87(3)
40	600	37.42(4)	40.49(5)	44.36(5)	47.91(4)

The solubility results of each isotherm are obtained by analyzing the density profiles of each simulation and averaging the densities of water and CO_2 in the aqueous phase (note that density profiles have been obtained by dividing the simulation box into 200–1000 slabs depending on the size of the simulation box). In order to calculate the solubility of CO_2 at the desired pressure value, it is necessary to fit the solubility results at each isotherm as a function of pressure, as we show in Fig. 2. From the graph, various conclusions can be drawn. First, and as expected from Henry's law, the solubility of CO_2 increases with increasing pressure. In addition, it is evident that lower temperatures result in higher solubility values (as expected in the case of gases, where solubility increases as temperature decreases). The obtained results align remarkably well with a linear fit, allowing us to accurately determine the solubilities

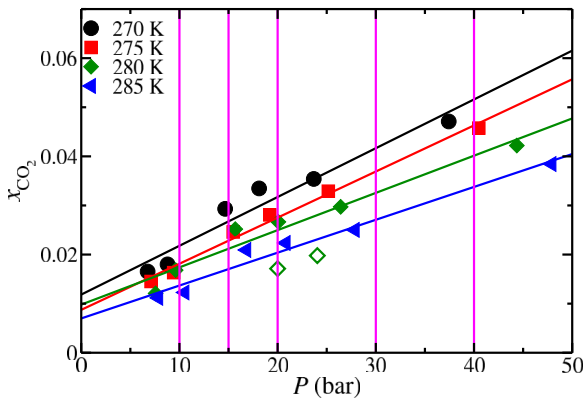

FIG. 2. Solubility of CO_2, as a function of pressure, for the four isotherms studied in this work in the aqueous phase when in contact via a planar interface with the vapor phase. The meaning of the symbols is explained in the legend. Magenta vertical lines represent the pressures chosen to interpolate the solubilities in this work. The black, red, green, and blue solid lines have been obtained by linearly fitting the solubility results at each temperature. The cross points between the magenta lines and each fitting line correspond to the solubility values used for the T_3 determination. Green open diamonds represent the experimental solubility of CO_2 taken from the literature[16,76] at 280 K and two different pressures.

of CO_2 at the desired pressure (marked as vertical magenta lines) for each of the studied isotherms. Unfortunately, the CO_2 solubility in the aqueous phase in contact with the vapor phase is slightly overestimated when compared with experimental data reported in the literature.[16,76] In particular, the simulated molar fraction is ~0.01 higher than the experimental value at 280 K, as shown in Fig. 2. This deviation arises from the use of the TIP4P/Ice water model and the chosen value of ξ, as previously discussed in Sec. II.

We now study the case of the H–L_{H_2O} equilibrium; since both are condensed phases, *NPT* anisotropic (where each box dimension can change independently) isobaric–isothermal simulations of 1200 ns have been carried out, where the first 400 ns are taken as the equilibration period and the last 800 ns as the production period—note that in this case, longer simulation times are required than in the V–L_{H_2O} *NVT* simulations because the dynamic of the solid hydrate phase is slower than that of the fluid phases. The H–L_{H_2O} simulation box consists of a hydrate composed of $4 \times 4 \times 4$ unit cells, corresponding to 2944 H_2O molecules and 512 CO_2 molecules, in contact with an aqueous phase containing 4000 H_2O molecules and 120 CO_2 molecules. A schematic view of the H–L_{H_2O} simulation setup is shown in the top-left snapshot of Fig. 1, where the hydrate phase (H), located on the left side of the simulation box, coexists across a planar interface with the water-rich liquid phase (L_{H_2O}) on the right. This system size, for both the hydrate phase and the aqueous phase, is sufficient to avoid finite-size effects and is consistent with the cutoff radius employed.[38,39,54] The temperature as well as the pressure can be kept constant by using the classic combination of a barostat plus a thermostat algorithm. The results obtained from the H–L_{H_2O} *NPT* anisotropic simulations are at the desired values of temperature (270, 275, 280, and 285 K) and pressure (10, 15, 20, 30, and 40 bar), and the density profiles can be used straightforwardly for solubility determination. In Fig. 3, we present first the solubility curves of H–L_{H_2O} (filled circles) at the five studied pressures. Interestingly, we observe that, similarly to the experiments,[16] at low temperatures, the highest pressure does not exhibit the highest solubility. Therefore, our results clearly agree with the experimental data. If we now plot the solubility curve V–L_{H_2O} as a function of temperature in Fig. 3, using the interpolations from the fits shown in Fig. 2 as previously described, we can determine the T_3 values for the five isobars under consideration. Under the three-phase coexistence conditions, the solubility obtained from both two-phase equilibria curves (V–L_{H_2O} and H–L_{H_2O}) should be the same. Thus, we obtain T_3 as the temperature at which the solubility isobars intersect each other on the graph. These intersection points are represented as crosses, each corresponding to the specific color of the respective isobar. As in the case of the aqueous phase in contact with the vapor phase, the CO_2 solubilities obtained for the aqueous solution when it is in contact with either the vapor or the hydrate phase are also slightly overestimated relative to experimental data reported in the literature.[16,76] In particular, the simulated molar fraction is about 0.01 higher than the experimental value at 280 K, as shown in Fig. 3. This deviation likewise stems from the use of the TIP4P/Ice water model and the chosen value of ξ, as discussed in Sec. II.

A separate issue concerns the level of agreement between our model predictions and experimental data from the literature. It is important to note that the combination of water and CO_2 models employed here, together with the chosen value of ξ, has been used previously by some of us to accurately predict the hydrate–liquid–liquid three-phase equilibrium of CO_2 hydrate at higher pressures.[23] Although this combination of the TIP4P/Ice water model, the CO_2 model, and the selected ξ value performs

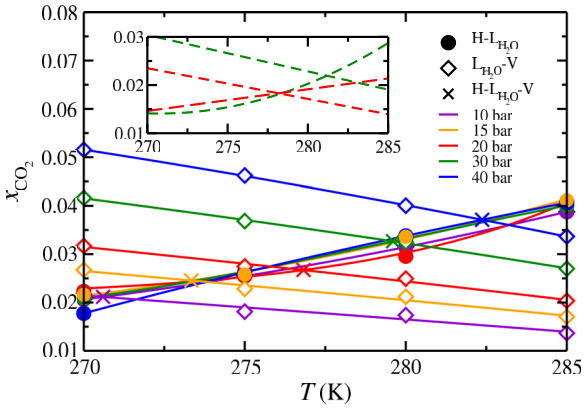

FIG. 3. Solubility of CO_2, as a function of temperature, at five pressures (10, 15, 20, 30, and 40 bar) of an aqueous phase when in contact via a planar interface with the vapor phase or the hydrate phase. The meaning of the symbols and lines in the main plot is represented in the legend. The red and green dashed curves shown in the inset correspond to correlations based on experimental data reported in the literature[16,76] for the solubilities of CO_2 in the aqueous solution when in contact with the vapor and hydrate phases along the isobars of 20 and 30 bar.

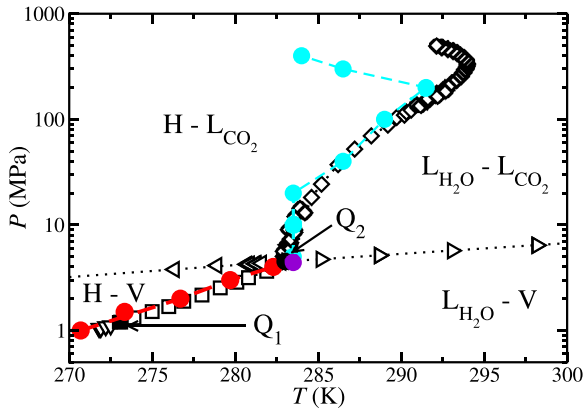

FIG. 4. Phase diagram of the CO_2 + water mixture assuming an excess of CO_2. The open black symbols represent the experimental three-phase lines for the H–L_{H_2O}–L_{CO_2} (diamonds),[10] H–L_{H_2O}–V (squares),[10] H–L_{CO_2}–V (left triangles),[10] L_{H_2O}–L_{CO_2}–V (right triangles),[10] and H–Ih–V (down triangles)[10] equilibria. The black-filled square and circle are the experimental quadruple points Q_1 and Q_2,[10] respectively. Cyan-filled circles correspond to simulation results obtained by some of us in a previous study[23] for the H–L_{H_2O}–L_{CO_2} three-phase line. Red-filled circles correspond to the three-phase line for the H–L_{H_2O}–V equilibrium obtained in this work. The violet-filled circle is the simulation quadruple point Q_2 obtained in this work. Note that the vapor phase consists mostly of CO_2 molecules as the vapor pressure of water is quite low at these temperatures. Similarly, the notation L_{H_2O}–L_{CO_2} focuses on the main component of each phase; however, some CO_2 molecules dissolve in L_{H_2O} and some water molecules dissolve in L_{CO_2}.

well for the H–L_{H_2O}–L_{CO_2} three-phase equilibrium, unfortunately it does not reproduce CO_2 solubilities with the same accuracy. The TIP4P/Ice model with $\xi = 1.13$ systematically overestimates experimental CO_2 solubilities. This deviation is not solely attributable to the value of ξ but is primarily due to intrinsic limitations of the water model. As shown in a recent study by some of us,[77] the overestimation originates from discrepancies between the TIP4P/Ice and experimental densities of pure water below 300 K. The physical origin of this overestimation lies in the water model. TIP4P/Ice predicts a liquid–water density that is systematically lower than the experimental one because it places the temperature of maximum density (TMD) at about 295 K instead of the experimental 277 K.[77] As a result, the model underestimates water density below 295 K, and this deviation persists over the pressure range relevant to the gas branch (1–50 bar). A reduced liquid density makes it easier for the aqueous phase to accommodate CO_2 molecules, lowering their chemical potential and thereby increasing the predicted solubility. The T_3 point corresponds to the temperature at which the solubility of CO_2 in the aqueous solution when it is in contact with the vapor phase becomes equal to that of CO_2 when it is in contact with the hydrate phase. Although our model overestimates the solubility of CO_2 in water when it is in equilibrium with the gas phase, it also overestimates the solubility when the aqueous phase is in equilibrium with the hydrate. As a result, the two curves intersect at a temperature close to the experimental T_3.

Indeed, once the three-phase equilibrium temperatures at different pressures have been calculated, we can encounter the challenge of constructing the phase diagram for pressures below 45 bar, where no previous equilibrium points were computed. The H–L_{H_2O}–L_{CO_2} line had been previously determined in several simulation studies,[23,26,28,38,39] but with this work, we are able for the first time to fill in the gaps in the phase diagram, which remain elusive in previous studies.

TABLE II. Three-phase coexistence temperatures, T_3, of CO_2 hydrate obtained from molecular simulations at different pressures P. Results for 10–40 bar (H–L_{H_2O}–V) are obtained in this work, whereas data for 50–4000 bar (H–L_{H_2O}–L_{CO_2}) were reported previously.[23] T_3^{exp} denotes the corresponding experimental values taken from the literature.[10] The last column lists the phases coexisting under the thermodynamic conditions of P and T_3.

P (bar)	T_3 (K)	T_3^{exp} (K)	Phases
10	271 (1)	⋯	H–L_{H_2O}–V[a]
15	273.3 (8)	274.8	H–L_{H_2O}–V
20	276.8 (8)	277.6	H–L_{H_2O}–V
30	279.6 (7)	280.3	H–L_{H_2O}–V
40	282.4 (8)	282.4	H–L_{H_2O}–V
50	284 (2)	282.9	H–L_{H_2O}–L_{CO_2}
100	284 (2)	283.6	H–L_{H_2O}–L_{CO_2}
200	284 (2)	284.6	H–L_{H_2O}–L_{CO_2}
400	287 (2)	286.2	H–L_{H_2O}–L_{CO_2}
1000	289 (2)	289.7	H–L_{H_2O}–L_{CO_2}
2000	292 (2)	293.0	H–L_{H_2O}–L_{CO_2}
3000	287 (2)	293.9	H–L_{H_2O}–L_{CO_2}
4000	284 (2)	293.6	H–L_{H_2O}–L_{CO_2}

[a]Notice that the simulation result obtained at 10 bar corresponds to a metastable point, and, hence, there is no experimental data for the H–L_{H_2O}–V equilibria at such pressure. Experimentally,[10] at 12.56 bar, there exists a quadrupole point (Q_1) where the CO_2 hydrate, an ice Ih, a water-rich liquid, and a vapor phase coexist. Under the Q_1 pressure, the water-rich liquid phase becomes unstable, and only three phases should coexist: CO_2 hydrate, ice Ih, and vapor.

Figure 4 shows the phase diagram of the CO_2–water mixture. The thermodynamic conditions corresponding to the H–L_{H_2O}–V and H–L_{H_2O}–L_{CO_2} three-phase equilibria are listed in Table II. The equilibrium line between the hydrate, liquid water, and liquid CO_2 phases was accurately reproduced, including the reentrant behavior, in previous MD simulations (cyan-filled circles) conducted by some of us[23] using the traditional three-phase direct coexistence technique. However, accessing the equilibrium line with the vapor phase (H–L_{H_2O}–V) was previously challenging. We now plot the calculations performed in this work (red-filled circles) for the equilibrium line with the vapor phase, using the solubility method, and remarkably, it aligns with the experimental line. This exciting development now allows us to calculate the quadruple point Q_2 as the intersection between our new calculations on the H–L_{H_2O}–V coexistence and those on the H–L_{H_2O}–L_{CO_2} coexistence. Our estimation of the Q_2 point (indicated by a violet circle in Fig. 4) is 283.5 K and 44 bar. Notably, this value agrees remarkably well (within the uncertainty) with the Q_2 measurement, which is reported as 283 K and 45 bar.[10] This strong agreement between our estimated quadruple point and experimental data reinforces the reliability of our methodology and the accuracy of the force field employed in this work.

IV. CONCLUSIONS

In this work, for the first time, computer simulations have successfully determined the three-phase coexistence equilibrium conditions of the CO_2 and water mixture. This achievement has been made possible by developing and applying a novel methodology based on solubility calculations, combined with previous DC simulations of condensed phases. Moreover, the successful alignment of our computed equilibrium lines with experimental data for both the H–L_{H_2O}–L_{CO_2} coexistence and the H–L_{H_2O}–V coexistence enables us to confidently estimate an upper quadruple point Q_2, which is in excellent agreement with experimental observations. Our findings demonstrate the significant advancements made in understanding the CO_2 and water mixture's phase behavior and provide valuable insights into the behavior of gas hydrates under different conditions. This methodology is expected to be applicable in the vapor region for other hydrates that exhibit an H–L_{H_2O}–V three-phase line, thereby paving the way for the systematic determination of additional hydrate dissociation lines. Such an extension would represent a significant step forward toward a more comprehensive understanding of hydrate phase behavior under low-pressure conditions.

ACKNOWLEDGMENTS

C.R.-G., J.A., and F.J.B. acknowledge Grant Nos. PID2021-125081NB-I00 and PID2024-158030NB-I00 funded by both MCIN/AEI/10.13039/501100011033 and FEDER EU and Universidad de Huelva (Grant No. P.O. FEDER EPIT1282023) and also co-funded by EU FEDER funds. M.M.C. also acknowledges Grant No. PID2022-136919NB-C32 funded by MCIN/AEI/10.13039/501100011033. C.R.-G. acknowledges the

FPI (Grant No. PRE2022-102927) from Ministerio de Ciencia e Innovación and Fondo Social Europeo Plus. C.V. also acknowledges Grant No. PID2022-136919NB-C31 funded by MCIN/AEI/10.13039/501100011033. We also greatly acknowledge RES resources provided by the Bioinnovation Center of the University of Malaga in Picasso to FI-2024-2-0030. The authors gratefully acknowledge the Universidad Politecnica de Madrid (www.upm.es) for providing computing resources on the Magerit Supercomputer. The authors would like to thank Carlos Vega in the Special Issue published in his honor. Working with him is truly a privilege, not only because of everything one learns, but also because even when you think you understand something perfectly, Carlos can ask a single question that makes you rethink everything, and somehow, he is always right. We look forward to continuing these discussions soon, ideally over a *Cocido Madrileño* and a *Vermut* at the Taberna de Ángel Sierra.

AUTHOR DECLARATIONS

Conflict of Interest

The authors have no conflicts to disclose.

Author Contributions

Jesús Algaba: Conceptualization (equal); Investigation (equal); Methodology (equal); Writing – original draft (equal); Writing – review & editing (equal). **Samuel Blazquez**: Investigation (equal); Methodology (equal); Writing – original draft (equal); Writing – review & editing (equal). **Cristóbal Romero-Guzmán**: Methodology (equal); Writing – review & editing (equal). **Carlos Vega**: Funding acquisition (equal); Methodology (equal); Writing – review & editing (equal). **María M. Conde**: Conceptualization (equal); Funding acquisition (equal); Methodology (equal); Writing – review & editing (equal). **Felipe J. Blas**: Conceptualization (equal); Funding acquisition (equal); Methodology (equal); Writing – review & editing (equal).

DATA AVAILABILITY

The data that support the findings of this study are available within the article.

REFERENCES

[1]S.-Y. Lee and G. D. Holder, "Methane hydrates potential as a future energy source," Fuel Process. Technol. **71**, 181–186 (2001).
[2]C. D. Ruppel and J. D. Kessler, "The interaction of climate change and methane hydrates," Rev. Geophys. **55**, 126–168, https://doi.org/10.1002/2016rg000534 (2017).
[3]H. P. Veluswamy, R. Kumar, and P. Linga, "Hydrogen storage in clathrate hydrates: Current state of the art and future directions," Appl. Energy **122**, 112–132 (2014).
[4]A. Hassanpouryouzband, J. Yang, B. Tohidi, E. Chuvilin, V. Istomin, B. Bukhanov, and A. Cheremisin, "CO_2 capture by injection of flue gas or CO_2–N_2 mixtures into hydrate reservoirs: Dependence of CO_2 capture efficiency on gas hydrate reservoir conditions," Environ. Sci. Technol. **52**, 4324–4330 (2018).
[5]Z. W. Ma, P. Zhang, H. S. Bao, and S. Deng, "Review of fundamental properties of CO_2 hydrates and CO_2 capture and separation using hydration method," Renewable Sustainable Energy Rev. **53**, 1273–1302 (2016).
[6]H. Dashti, L. Z. Yew, and X. Lou, "Recent advances in gas hydrate-based CO_2 capture," J. Nat. Gas Sci. Eng. **23**, 195–207 (2015).
[7]S. F. Cannone, A. Lanzini, and M. Santarelli, "A review on CO_2 capture technologies with focus on CO_2-enhanced methane recovery from hydrates," Energies **14**, 387 (2021).
[8]N. H. Duc, F. Chauvy, and J.-M. Herri, "CO_2 capture by hydrate crystallization–A potential solution for gas emission of steelmaking industry," Energy Convers. Manage. **48**, 1313–1322 (2007).
[9]W. Choi, J. Mok, J. Lee, Y. Lee, J. Lee, A. K. Sum, and Y. Seo, "Effective CH_4 production and novel CO_2 storage through depressurization-assisted replacement in natural gas hydrate-bearing sediment," Appl. Energy **326**, 119971 (2022).
[10]E. D. Sloan and C. Koh, *Clathrate Hydrates of Natural Gases*, 3rd ed. (CRC Press, New York, 2008).
[11]J. A. Ripmeester and S. Alavi, *Clathrate Hydrates: Molecular Science and Characterization* (Wiley-VCH, Weinheim, Germany, 2022).
[12]H. Lee, J.-W. Lee, D. Y. Kim, J. Park, Y.-T. Seo, H. Zeng, I. L. Moudrakovski, C. I. Ratcliffe, and J. A. Ripmeester, "Tuning clathrate hydrates for hydrogen storage," Nature **434**, 743–746 (2005).
[13]K. A. Lokshin, Y. Zhao, D. He, W. L. Mao, H.-K. Mao, R. J. Hemley, M. V. Lobanov, and M. Greenblatt, "Structure and dynamics of hydrogen molecules in the novel clathrate hydrate by high pressure neutron diffraction," Phys. Rev. Lett. **93**, 125503 (2004).
[14]L. Yi, X. Zhou, Y. He, Z. Cai, L. Zhao, W. Zhang, and Y. Shao, "Molecular dynamics simulation study on the growth of structure ii nitrogen hydrate," J. Phys. Chem. B **123**, 9180–9186 (2019).
[15]B. R. Lee, C. A. Koh, and A. K. Sum, "Quantitative measurement and mechanisms for CH_4 production from hydrates with the injection of liquid CO_2," Phys. Chem. Chem. Phys. **16**, 14922–14927 (2014).
[16]P. Servio and P. Englezos, "Effect of temperature and pressure on the solubility of carbon dioxide in water in the presence of gas hydrate," Fluid Phase Equilib. **190**, 127–134 (2001).
[17]A. K. Sum, R. C. Burruss, and E. D. Sloan, "Measurement of clathrate hydrates via Raman spectroscopy," J. Phys. Chem. B **101**, 7371–7377 (1997).
[18]T. Makiya, T. Murakami, S. Takeya, A. K. Sum, S. Alavi, and R. Ohmura, "Synthesis and characterization of clathrate hydrates containing carbon dioxide and ethanol," Phys. Chem. Chem. Phys. **12**, 9927–9932 (2010).
[19]J. C. Cordeiro, Jr., M. A. Marcelino Neto, R. E. M. Morales, and A. K. Sum, "Phase equilibrium of carbon dioxide hydrates inhibited with MEG and NaCl above the upper quadruple point," J. Chem. Eng. Data **65**, 280–286 (2019).
[20]D.-Y. Koh, H. Kang, D.-O. Kim, J. Park, M. Cha, and H. Lee, "Recovery of methane from gas hydrates intercalated within natural sediments using CO_2 and a CO_2/N_2 gas mixture," ChemSusChem **5**, 1443–1448 (2012).
[21]M. Pan, N. A. Ismail, M. Luzi-Helbing, C. A. Koh, and J. M. Schicks, "New insights on a μm-scale into the transformation process of CH_4 hydrates to CO_2-rich mixed hydrates," Energies **13**, 5908 (2020).
[22]D. Daniel-David, F. Guerton, C. Dicharry, J.-P. Torré, and D. Broseta, "Hydrate growth at the interface between water and pure or mixed CO_2/CH_4 gases: Influence of pressure, temperature, gas composition and water-soluble surfactants," Chem. Eng. Sci. **132**, 118–127 (2015).
[23]J. M. Míguez, M. M. Conde, J.-P. Torré, F. J. Blas, M. M. Piñeiro, and C. Vega, "Molecular dynamics simulation of CO_2 hydrates: Prediction of three phase coexistence line," J. Chem. Phys. **142**, 124505 (2015).
[24]M. Pérez-Rodríguez, A. Vidal-Vidal, J. Míguez, F. J. Blas, J.-P. Torré, and M. M. Piñeiro, "Computational study of the interplay between intermolecular interactions and CO_2 orientations in type I hydrates," Phys. Chem. Chem. Phys. **19**, 3384–3393 (2017).
[25]M. H. Waage, T. J. H. Vlugt, and S. Kjelstrup, "Phase diagram of methane and carbon dioxide hydrates computed by Monte Carlo simulations," J. Phys. Chem. B **121**, 7336–7350 (2017).
[26]J. Costandy, V. K. Michalis, I. N. Tsimpanogiannis, A. K. Stubos, and I. G. Economou, "The role of intermolecular interactions in the prediction of the phase equilibria of carbon dioxide hydrates," J. Chem. Phys. **143**, 094506 (2015).
[27]Y. Zhang, L. Zhao, S. Deng, X. Nie, and Z. Du, "Molecular dynamics simulation on carbon dioxide hydrate formation," Energy Procedia **158**, 4648–4654 (2019).
[28]J. Algaba, I. M. Zerón, J. M. Míguez, J. Grabowska, S. Blazquez, E. Sanz, C. Vega, and F. J. Blas, "Solubility of carbon dioxide in water: Some useful results for hydrate nucleation," J. Chem. Phys. **158**, 184703 (2023).

[29]M. Pineda, A. Phan, C. A. Koh, A. Striolo, and M. Stamatakis, "Stochastic cellular automata modeling of CO_2 hydrate growth and morphology," Cryst. Growth Des. **23**, 4222–4239 (2023).
[30]B. C. Barnes and A. K. Sum, "Advances in molecular simulations of clathrate hydrates," Curr. Opin. Chem. Eng. **2**, 184–190 (2013).
[31]A. Phan, H. Schlösser, and A. Striolo, "Molecular mechanisms by which tetrahydrofuran affects CO_2 hydrate growth: Implications for carbon storage," Chem. Eng. J. **418**, 129423 (2021).
[32]P.-W. Wang, D. T. Wu, and S.-T. Lin, "Promotion mechanism for the growth of CO_2 hydrate with urea using molecular dynamics simulations," Chem. Commun. **57**, 5330–5333 (2021).
[33]L. C. Jacobson, W. Hujo, and V. Molinero, "Nucleation pathways of clathrate hydrates: Effect of guest size and solubility," J. Phys. Chem. B **114**, 13796–13807 (2010).
[34]L. C. Jacobson, W. Hujo, and V. Molinero, "Amorphous precursors in the nucleation of clathrate hydrates," J. Am. Chem. Soc. **132**, 11806–11811 (2010).
[35]G. Román-Pérez, M. Moaied, J. M. Soler, and F. Yndurain, "Stability, adsorption, and diffusion of CH_4, CO_2, and H_2 in clathrate hydrates," Phys. Rev. Lett. **105**, 145901 (2010).
[36]I. M. Zerón, J. Algaba, J. M. Míguez, J. Grabowska, S. Blazquez, E. Sanz, C. Vega, and F. J. Blas, "Homogeneous nucleation rate of carbon dioxide hydrate formation under experimental condition from seeding simulations," J. Chem. Phys. **162**, 134708 (2025).
[37]C. Romero-Guzmán, I. M. Zerón, J. Algaba, B. Mendiboure, J. M. Míguez, and F. J. Blas, "Effect of pressure on the carbon dioxide hydrate–water interfacial free energy along its dissociation line," J. Chem. Phys. **158**, 194704 (2023).
[38]J. Algaba, S. Blazquez, E. Feria, J. M. Míguez, M. M. Conde, and F. J. Blas, "Three-phase equilibria of hydrates from computer simulation. II. Finite-size effects in the carbon dioxide hydrate," J. Chem. Phys. **160**, 164722 (2024).
[39]J. Algaba, S. Blazquez, J. M. Míguez, M. M. Conde, and F. J. Blas, "Three-phase equilibria of hydrates from computer simulation. III. Effect of dispersive interactions in the methane and carbon dioxide hydrates," J. Chem. Phys. **160**, 164723 (2024).
[40]M. P. Allen and D. J. Tildesley, *Computer Simulation of Liquids*, 2nd ed. (Claredon, Oxford, 2017).
[41]D. Frenkel and B. Smit, *Understanding Molecular Simulations*, 2nd ed. (Academic, San Diego, 2002).
[42]A. J. C. Ladd and L. V. Woodcock, "Triple-point coexistence properties of the Lennard-Jones system," Chem. Phys. Lett. **51**, 155–159 (1977).
[43]A. J. C. Ladd and L. V. Woodcock, "Interfacial and co-existence properties of the Lennard-Jones system at the triple point," Mol. Phys. **36**, 611–619 (1978).
[44]M. M. Conde and C. Vega, "Determining the three-phase coexistence line in methane hydrates using computer simulations," J. Chem. Phys. **133**, 064507 (2010).
[45]M. M. Conde and C. Vega, "Note: A simple correlation to locate the three phase coexistence line in methane-hydrate simulations," J. Chem. Phys. **138**, 056101 (2013).
[46]L. Jensen, K. Thomsen, N. von Solms, S. Wierzchowski, M. R. Walsh, C. A. Koh, E. D. Sloan, D. T. Wu, and A. K. Sum, "Calculation of liquid water–hydrate–methane vapor phase equilibria from molecular simulations," J. Phys. Chem. B **114**, 5775–5782 (2010).
[47]V. K. Michalis, J. Costandy, I. N. Tsimpanogiannis, A. K. Stubos, and I. G. Economou, "Prediction of the phase equilibria of methane hydrates using the direct phase coexistence methodology," J. Chem. Phys. **142**, 044501 (2015).
[48]A. M. Fernández-Fernández, M. Pérez-Rodríguez, A. Comesaña, and M. M. Piñeiro, "Three-phase equilibrium curve shift for methane hydrate in oceanic conditions calculated from molecular dynamics simulations," J. Mol. Liq. **274**, 426–433 (2019).
[49]A. M. Fernández-Fernández, M. M. Piñeiro, and M. Pérez-Rodríguez, "Molecular dynamics of fluoromethane type I hydrates," J. Mol. Liq. **339**, 116720 (2021).
[50]Á. M. Fernández-Fernández, M. M. Conde, G. Pérez-Sánchez, M. Pérez-Rodríguez, and M. M. Piñeiro, "Molecular simulation of methane hydrate growth confined into a silica pore," J. Mol. Liq. **362**, 119698 (2022).
[51]S. Blazquez, C. Vega, and M. M. Conde, "Three phase equilibria of the methane hydrate in NaCl solutions: A simulation study," J. Mol. Liq. **383**, 122031 (2023).
[52]A. Borrero, A. Díaz-Acosta, S. Blazquez, I. M. Zerón, J. Algaba, M. M. Conde, and F. J. Blas, "Three-phase equilibria of CO_2 hydrate from computer simulation in the presence of NaCl," Energy Fuels **39**, 5522–5533 (2025).
[53]M. J. Torrejón, S. Blazquez, J. Algaba, M. M. Conde, and F. J. Blas, "Dissociation line and driving force for nucleation of the multiple occupied hydrogen hydrate from computer simulation," Energy Fuels **39**, 15184–15197 (2025).
[54]S. Blazquez, J. Algaba, J. M. Míguez, C. Vega, F. J. Blas, and M. M. Conde, "Three-phase equilibria of hydrates from computer simulation. I. Finite-size effects in the methane hydrate," J. Chem. Phys. **160**, 164721 (2024).
[55]J. Algaba, C. Romero-Guzmán, M. J. Torrejón, and F. J. Blas, "Prediction of the univariant two-phase coexistence line of the tetrahydrofuran hydrate from computer simulation," J. Phys. Chem. **160**, 164718 (2024).
[56]H. Tanaka, T. Yagasaki, and M. Matsumoto, "On the thermodynamic stability of clathrate hydrates VI: Complete phase diagram," J. Phys. Chem. B **122**, 297–308 (2018).
[57]L. F. Vega and F. J. Blas, "Tricritical phenomena in chain-like mixtures from a molecular-based equation of state," Fluid Phase Equilib. **171**, 91–104 (2000).
[58]J. M. Míguez, M. C. dos Ramos, M. M. Piñeiro, and F. J. Blas, "An examination of the ternary methane + carbon dioxide + water phase diagram using the SAFT-VR approach," J. Phys. Chem. B **115**, 9604–9617 (2011).
[59]J. M. Míguez, M. M. Piñeiro, J. Algaba, B. Mendiboure, J. P. Torré, and F. J. Blas, "Understanding the phase behavior of tetrahydrofuran + carbon dioxide, + methane, and + water binary mixtures from the SAFT-VR approach," J. Phys. Chem. B **119**, 14288–14302 (2015).
[60]J. Grabowska, S. Blázquez, E. Sanz, I. M. Zerón, J. Algaba, J. M. Míguez, F. J. Blas, and C. Vega, "Solubility of methane in water: Some useful results for hydrate nucleation," J. Phys. Chem. B **126**, 8553–8570 (2022).
[61]J. Algaba, M. J. Torrejón, and F. J. Blas, "Dissociation line and driving force for nucleation of the nitrogen hydrate from computer simulation," J. Chem. Phys. **159**, 224707 (2023).
[62]M. J. Torrejón, J. Algaba, and F. J. Blas, "Dissociation line and driving force for nucleation of the nitrogen hydrate from computer simulation. II. Effect of multiple occupancy," J. Chem. Phys. **161**, 054712 (2024).
[63]H. Tanaka, M. Matsumoto, and T. Yagasaki, "On the phase behaviors of CH_4–CO_2 binary clathrate hydrates: Equilibrium with aqueous phase," J. Chem. Phys. **161**, 214503 (2024).
[64]H. Tanaka, M. Matsumoto, T. Yagasaki, M. Takeuchi, Y. Mori, and T. Kono, "The solubilities of water in liquid CO_2 coexisting with water or hydrate," J. Chem. Phys. **163**, 124504 (2025).
[65]J. C. Platteeuw and J. H. van der Waals, "Thermodynamic properties of gas hydrates," Mol. Phys. **1**, 91–96 (1958).
[66]J. C. Platteeuw and J. H. V. der Waals, "Thermodynamic properties of gas hydrates II: Phase equilibria in the system H_2S-C_3H_3-H_2O at −3°C," Recl. Trav. Chim. Pays-Bas **78**, 126–133 (1959).
[67]S. Marchio, S. Meloni, A. Giacomello, C. Valeriani, and C. M. Casciola, "Pressure control in interfacial systems: Atomistic simulations of vapor nucleation," J. Chem. Phys. **148**, 064706 (2018).
[68]J. L. F. Abascal, E. Sanz, R. G. Fernández, and C. Vega, "A potential model for the study of ices and amorphous water: TIP4P/Ice," J. Chem. Phys. **122**, 234511 (2005).
[69]J. J. Potoff and J. I. Siepmann, "Vapor–liquid equilibria of mixtures containing alkanes, carbon dioxide, and nitrogen," AIChE J. **47**, 1676–1682 (2001).
[70]D. van der Spoel, E. Lindahl, B. Hess, G. Groenhof, A. E. Mark, and H. J. C. Berendsen, "Gromacs: Fast, flexible, and free," J. Comput. Chem. **26**, 1701–1718 (2005).
[71]M. A. Cuendet and W. F. V. Gunsteren, "On the calculation of velocity-dependent properties in molecular dynamics simulations using the leapfrog integration algorithm," J. Chem. Phys. **127**, 184102 (2007).
[72]U. Essmann, L. Perera, M. L. Berkowitz, T. Darden, H. Lee, and L. G. Pedersen, "A smooth particle mesh Ewald method," J. Chem. Phys. **103**, 8577–8593 (1995).

[73]L. Lundberg and O. Edholm, "Dispersion corrections to the surface tension at planar surfaces," J. Chem. Theory Comput. **12**, 4025–4032 (2016).
[74]S. Nosé, "A molecular dynamics method for simulations in the canonical ensemble," Mol. Phys. **52**, 255–268 (1984).
[75]M. Parrinello and A. Rahman, "Polymorphic transitions in single crystals: A new molecular dynamics method," J. Appl. Phys. **52**, 7182–7190 (1981).
[76]X.-H. Wang, Y.-W. Wu, Z.-B. Xu, T.-H. Zhang, L. Zhao, H.-S. Wang, L.-Y. Bao *et al.*, "CO_2 solubility in aqueous solution in a hydrate-liquid two-phase equilibrium system," Ind. Eng. Chem. Res. **64**, 11596–11604 (2025).
[77]S. Blazquez, M. M. Conde, and C. Vega, "Solubility of CO_2 in salty water: Adsorption, interfacial tension and salting out effect," Mol. Phys. **122**, e2306242 (2024).